(Received 24 June 2024, Accepted 4 August 2024, Scheduled 18 November 2024)

Slot Antenna in Cylindrical Coupling Brick for Microwave Brain Imaging

Antonio Cuccaro[1,*], Angela Dell'Aversano[2], Bruno Basile[3], and Raffaele Solimene[2]

[1] *DIMES-University of Calabria, Rende (CS), Italy*
[2] *Dipartimento di Ingegneria, Universitá della Campania — L.Vanvitelli, Aversa, Italy*
[3] *TTC Medical S.r.l, Casalnuovo di Napoli, Italy*

ABSTRACT: In this contribution, two antennas for microwave imaging are described and validated. The first solution is a slot antenna designed when it works a direct contact with human head. However, the air-gap issues and hair layer degrade the antenna performances. These limitations are overcome with the cylindrical brick antenna containing coupling liquid medium. Basically, this antenna consists of a ground plane hosting a wide slot and a microstrip feed line with a fork-like tuning stub inserted within the circular container. Numerical examples show that the proposed antenna exhibits S_{11} below -10 dB over the selected frequency band from 1 to 2 GHz, in agreement with microwave brain imaging systems. Moreover, the antenna is assessed in terms of transmission coefficients and field penetration. In particular, it is shown that such a feature holds true when the antenna is placed in different positions over the head, when it is located on both the skin and hair. Experiments on a few real humans confirm the numerical results. The transmission coefficient, which is the only one used in imaging systems to streamline the hardware complexity, is of comparable level of other similar antennas already present in literature. However, the proposed antenna is lighter and smaller in size.

1. INTRODUCTION

Microwave imaging (MWI) is emerging as a promising tool that can potentially supplement other well-assessed imaging modalities in medical diagnostics [1]. Most of the pertinent literature focuses on breast cancer imaging [2–6]. However, other biomedical diagnostic areas have also been explored recently [7, 8]. This paper deals with MWI for brain diagnostics. In this framework, the book by Crocco et al. [9] gives a detailed and useful account of recent developments in electromagnetic technologies exploited in brain diseases diagnostics and monitoring. In particular, those scholars highlight how MWI is potentially able to address the two main issues related to stroke diagnosis and management. One is the possibility to achieve early pre-hospital diagnosis, which is hardly feasible by magnetic resonance imaging (MRI) and computer tomography (CT), since transporting MRI or CT machines (which are very bulky) in an ambulance is currently unrealistic; the other one is the possibility of a continuous brain monitoring for stroke in the post-acute stage.

The mentioned potential advantages have triggered extensive research into the development of portable medical diagnostic systems, both in terms of the processing algorithms to get the images and the achievement of reduced complexity hardware and component miniaturization.

In MWI system, antenna plays a major role since it is the hardware component with which the system interacts with the scene under test. Therefore, the design of the antenna is of paramount importance. This is even more true in biomedical applications, where the antenna is often asked to work in contact with the object under test. Indeed, the way the antenna radiates, the radiated power, and its frequency band affect the penetration depth inside the human head, the signal-to-noise ratio (SNR), and the frequency band of the data supplied to imaging algorithms. It is clear then that there are several issues to address when designing an antenna, especially in biomedical applications (see Fig. 1). Accordingly, here, the question that it deals with concerns how to choose the antenna type in brain imaging in order to satisfy the features described above. In particular, attention is paid to the compactness constraint that is suitable for a portable microwave device.

Many different types of antennas have been considered for biomedical MWI. For example, in [10] a wide-band system is considered to obtain high resolution images. An ultra-wideband (UWB) multiple-input multiple-output (MIMO) probe is proposed in [11] for tumor detection in breast. Similar UWB antennas are proposed in [12] and [13] for stroke detection. In particular, in [13] an antenna is proposed for implantable head applications, while an implantable narrow-band antenna for brain machine interface is proposed in [14]. In [15] a band about 2 GHz is used for fast diagnosis of medical emergencies pertaining to brain injuries. Frequency modulated continuous waves (FMCWs) are employed in [16], where a non-contact system and an automatic recognition algorithm for stroke detection are proposed. However, in general, the antenna frequency band should be devised by taking into account the chosen imaging algorithm and the physics of the problem. Regarding the brain imaging, the antennas can be categorized in two broad categories: radiators that work away

* Corresponding author: Antonio Cuccaro (antonio.cuccaro@unical.it).

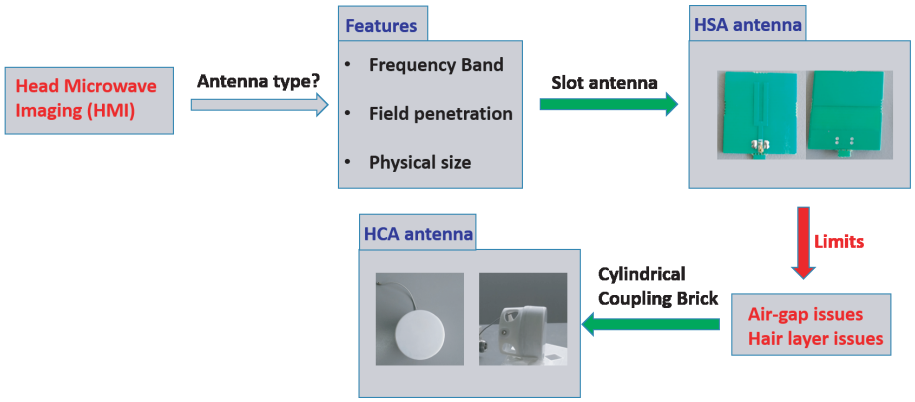

FIGURE 1. Block diagram for the selected antennas.

from the head and those that work in contact with it. For the latter antenna class, usually the radiators are designed by considering the perfect physical matching between it and the skin layer of the head model. However, no one has addressed (to the authors' knowledge) the practical aspect regarding the hair effect on the antenna performance or how its behavior changes due to head curvature and accordingly when partial air gap occurs. Both aspects are addressed in the paper. Moreover, for brain imaging, the study reported in [17] has shown that frequencies around 1 GHz give a good trade-off between penetration depth and resolution.

A way to improve penetration depth in human tissues, and at the same time to reduce the size of the antenna, is to immerse the antenna into a coupling medium [18], which is used to smooth the jump in the electromagnetic properties that electromagnetic waves experience while penetrating into the body. This solution, though very simple, can be inconvenient in the prospective of portable and compact devices.

A coupling medium is not necessary when antennas are designed to work on-body. In [19], a compact 4×4 wide-band array is proposed to work in direct contact with the breast skin. Following the same concept, a planar structure is proposed in [20] and [21], where a flexible array system is considered. An important aspect to consider when the array is employed in microwave imaging system is mutual coupling. If this phenomenon is not properly taken into account, the results of exam can be compromised. Accordingly, some mutual coupling reducing strategies are needed as shown in [22]. Obviously, antennas designed to work in free-space do not efficiently work when being put in contact with biological tissues [23].

While the major benefits of antennas-on-skin are practically the same as antennas working in coupling media, there are two main issues to be properly addressed. The first one concerns the fact that, even though the antenna is designed by possibly taking into account the tissues of the region under test, when it is attached to the head (or to any other part of human body), its behavior becomes unknown or known with some degree of uncertainty. This is because tissues' features are not exactly known, and they are not the same for different patients and can change even by considering different body parts of the same patient. This can be a drawback for imaging algorithms. However, by employing non-coherent imaging strategies the uncertainty about the antenna's behavior is mitigated [24]. The other question is that a good physical contact between antenna and skin must be ensured, since even thin air-gaps can dramatically change the antenna's response.

To cope with this issue, one option is to reduce the size of the antennas so as to make the deployment less sensitive to the head curvature. A different strategy has been presented in [25], where the proposed antenna consists of a brick of semi-flexible custom-made material in which the antenna is embedded. In this way, all the advantages of using a coupling medium are preserved (without the need of a coupling liquid around the head), and the effect of air gap is strongly mitigated. However, the antenna's volume can put a constraint on the array's size in terms of the number of different sensors that can be deployed in the scene.

In this paper, both of the above mentioned strategies are considered and compared. To this end, two antenna types conceived to work in contact with the head are designed, for head diagnostics. The first antenna is a slot that exploits the loading effect of the head to get size reduction and hence to mitigate air-gap effect. It is shown that such an antenna performs well as long as it is located on the head skin. However, performance degrades when the antenna is located over the hair. This suggests that hair effect must be properly taken into account so that the antenna can work well both when it is located on the skin and on the hair. This quite obvious consideration seems to be not properly considered in literature. To cope with this issue, a second antenna is proposed. More in detail, the previous antenna is optimized to work when being immersed in a coupling liquid contained in a small cylindrical container. While the idea is similar to the one exploited in [25], the obtained antenna is easy to fabricate, smaller in size, and presents a relatively stable response when working in contact to the skin and the hair layer.

The rest of the paper is organized as follows. Sections 2 and 3 introduce head slot antenna (HSA) and head circular antenna (HCA), respectively. Both solutions are validated with numerical experiments, and the prototypes realizations are shown. In Section 4, a numerical phantom derived from magnetic resonance imaging MRI is employed for validate the HSA and HCA against more realistic scenario. Section 5 gives the experimental results. Finally, the conclusions are given in Section 6.

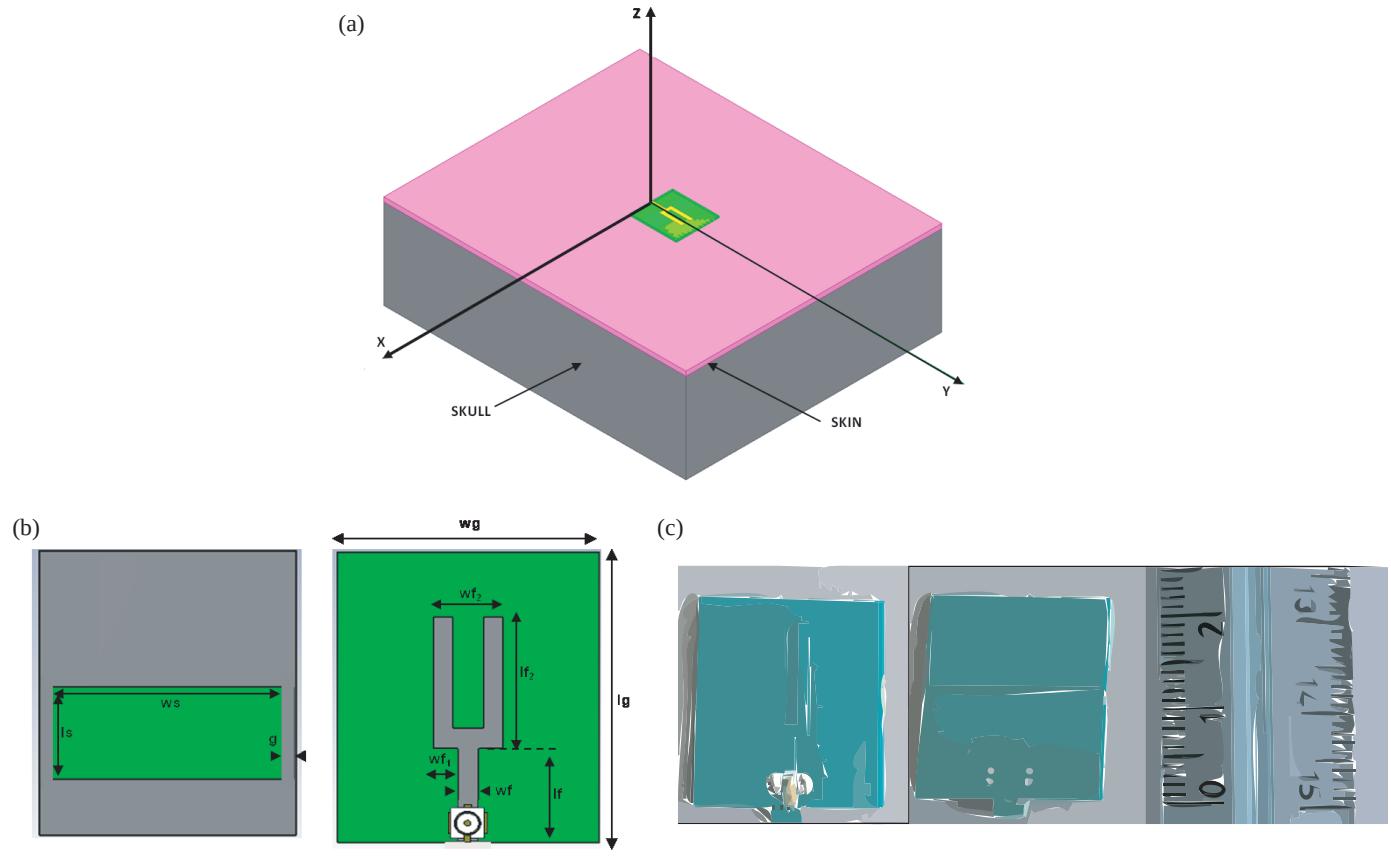

FIGURE 2. Pictorial view of the antenna and the simplified two-layered phantom used during the design stage. Panel (a) shows the two-layered planar simplified head phantom, (b) top and side views on the antenna plane, and (c) antenna prototype.

2. SLOT ANTENNA DESIGN, REALIZATION AND NUMERICAL RESULTS

In order to create a compact and transportable diagnostic stroke detection system, the use of a miniaturized antenna is certainly desirable. This can be achieved in a number of ways, for example adopting planar antennas with high permittivity substrates or inserting the antenna into a coupling medium.

Herein, instead, the antenna is designed to be directly attached to the human head. To this end, according to detailed studies on aperture antenna irradiation [26–28], a wide slot antenna is considered for our purposes. Indeed, this solution fits well with the need of compactness and lightness.

The designed antenna is then a slot antenna printed on a standard FR4 substrate (thickness $h_s = 0.8\,\text{mm}$, $\epsilon_r = 4.4$ and $\sigma = 0.012\,\text{S/m}$). The antenna is designed to be compact and contained within a virtual surface of 2 cm in diameter, and according to [17], to work in the $[1, 2]\,\text{GHz}$ frequency band. Moreover, in order to improve the ability of the antenna to radiate into the phantom, a minimum return loss of 10 dB, across the operating frequency band, is required. Basically, the antenna consists of two elements: the ground plane which hosts the wide slot and a microstrip feed line with a fork-like tuning stub. By properly selecting the parameters of the fork-feed, the coupling between the microstrip and wide slot can be controlled. This can help in enhancing the operative bandwidth. Moreover, to facilitate the antenna's positioning on the human head, a micro-SMA connector is placed on the side where the fork-feed is present (see Fig. 2(b)).

To design an antenna that has to work in contact with the head, a model of the head must be taken into account during the design and the subsequent optimization stages. This is not a serious problem since numerical head models are easily available. The point is that having chosen a model this in general will be different from the actual head under operative conditions. For example, head curvature as well as actual tissue layering changes from patient to patient.

Therefore, here, a different approach is followed. In particular, the first two layers of a human head are for sure skin and skull. Also, in view of the targeted antenna's small size, the air/head interface can be considered locally flat. Accordingly, the antenna is designed and optimized to work in contact with the simplified two-layered head phantom shown in Fig. 2(a). In particular, both skin and skull tissues are considered homogeneous and lossless. The skin layer has thickness $t_{skin} = 2.0\,\text{mm}$ and permittivity $\epsilon_{r-skin} = 36$, whereas the skull layer has a permittivity $\epsilon_{r-skull} = 15$ [17], and its thickness is set to be very large (150 mm) so that it can be considered unbounded along z. The final geometrical dimensions of the designed slot antenna are listed in Table 1, whereas the prototype is show in Fig. 2(c). In the sequel, this antenna will be denoted as HSA, which stands for head slot antenna.

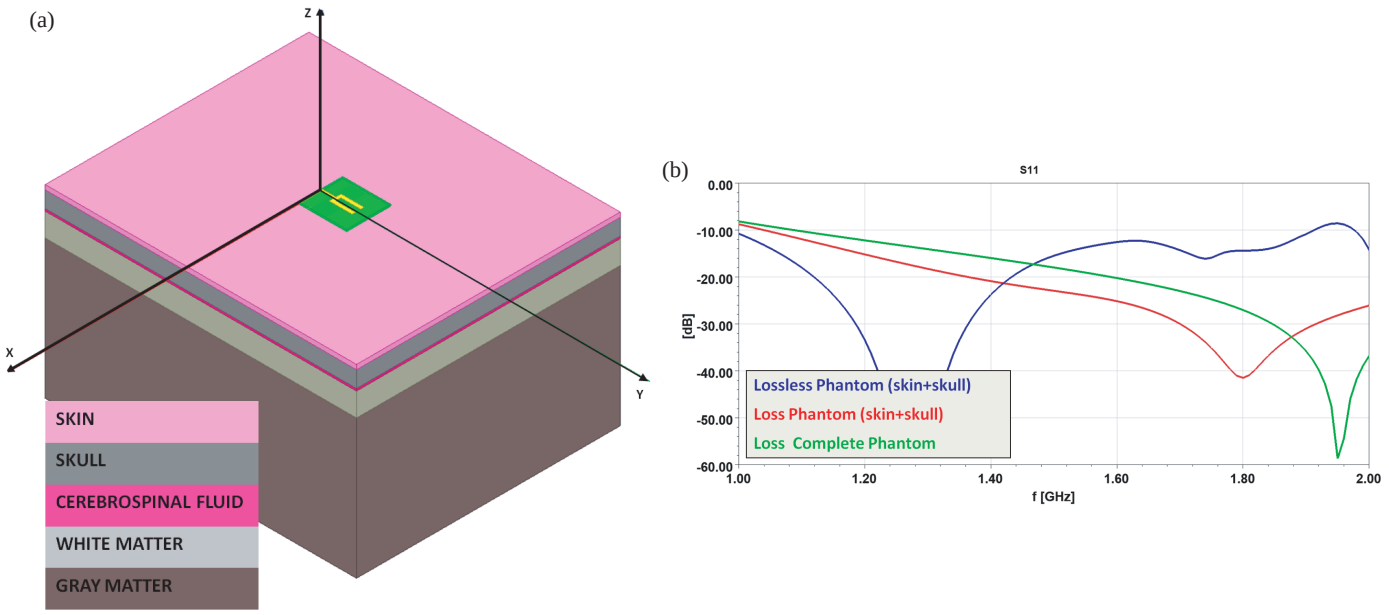

FIGURE 3. Checking the designed antenna. Panel (a) shows five-layered phantom (complete phantom), and (b) S_{11} behaviours pertaining to the two-layered phantom without losses (blue line) and with losses (red line), and to the complete phantom (green line).

TABLE 1. Dimensions of designed HSA.

Label	Value [mm]	Label	Value [mm]
wf	0.81	lf_2	10.00
wg	19.00	lg	20.70
wf_1	2.21	lf	6.17
wf_2	5.22	g	0.39
ws	18.22	ls	6.93

It is once again remarked that a more involved numerical phantom could have been considered during the design stage. However, as pointed out above, the simplified phantom is considered as in Fig. 2(a) because the actual layering and tissues properties are actually unknown. The point is to check how this uncertainty affects the antenna's response. This crucial question is addressed later.

Finally, it is noted that the area of the front (radiating) part of the proposed slot antenna is very small compared to an antenna working in free-space at same frequency band, about 2 cm $\times$2 cm. Now, by considering that the average area of the upper part of a human head is approximately 1000 cm^2 [25], it is clear that the number of antennas that can be deployed on the head is about two hundred. Accordingly, the number of antennas certainly is not a constraint, but instead could be useful for improving the SNR system. Also, when the antenna is designed to work in contact with head, effectively the head curvature can be a serious issue. This can be explained by reasoning in terms of loading effect. Indeed, in principle, the head can be modeled as a load for the antenna. Our antenna is designed taking account this loading effect. Accordingly, every change of the load affects the antennas performance. When the head curvature ensures a perfect contact between antenna and skin, the load changes are little; therefore, the antenna performance remains stable. Things dramatically change if the head curvature allows only partial contact between the antenna and the skin. The non-perfect contact causes relevant load changes; therefore, the antenna performance degrades. However, in view of such a reduced antenna size, head curvature should not be a serious issue since it is a quasi-plane from the antenna's point of view.

The antenna's behaviour, through numerical simulations by considering the antenna scattering parameters S_{11}, is checked.

In order to get the numerical examples, the HFSS Ansys software is exploited. The first issue is to check the antenna's response when it is located over a phantom which does not coincide with the one employed during the design stage. To this end, a more complex (still planar) phantom consisting of five layers mimicking skin, skull, cerebrospinal fluid, white matter (WM), and grey matter (GM) tissues, respectively, (see Fig. 3(a)) is considered. In order to distinguish this phantom from the two-layered phantom, the five-layered phantom is named as a complete phantom. The properties of the tissues used in the simulations come from [29] and reported in Table 2 at the frequency of 1 GHz. Note that the properties of the skin and skull layers have been changed with respect to the ones employed in the two-layered phantom used for the antenna design. Fig. 3(b) reports the S_{11} behaviour over the selected operative frequency band when the antenna is in contact with a two-layered phan-

TABLE 2. Tissues's properties at 1 GHz.

Tissue	Skin	Bone	CSF	WM	GM
ϵ_r	41	18	68.2	35.58	52.30
σ [S/m]	0.85	0.40	2.30	0.62	0.98
Tickness [mm]	2	7	1	10	50

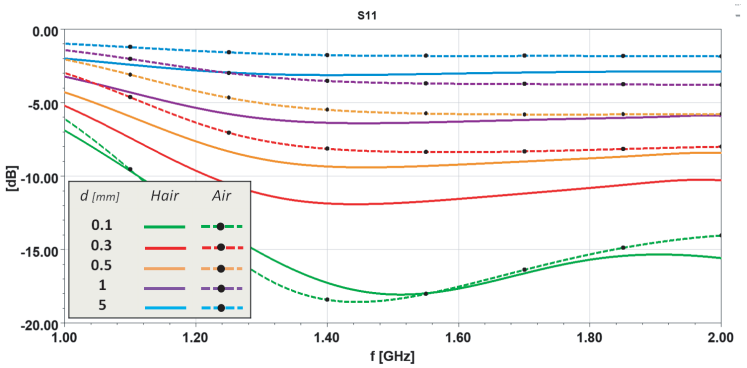

FIGURE 4. HSA S_{11} for different air-gap and hair thicknesses. The same phantom as in Fig. 3(a) is considered with air-gap and hair layer between antenna and skin.

tom. In particular, the blue line refers to the lossless phantom displayed in Fig. 2, whereas the red line is still relative to a two-layered phantom, but the skin and skull parameters are taken from Fig. 3(b) (hence, with losses). Finally, the green line pertains to the complete phantom. As expected, since the slot HSA is strongly subject to the loading effect of the phantom [26, 28], the resonances of S_{11} result shifted. However, what matters is that the constraints on the return loss holds true since in all the cases S_{11} are below -10 dB, practically across the whole operative frequency band.

As mentioned above, one of the critical issues for antennas designed to work in contact with the head is air gaps that could form during antenna positioning. In this framework, it is natural to expect that even the hair can have an impact on the antenna's response. Nonetheless, to the best of authors' knowledge, no papers have investigated the role of hair. To cope with this lack, the antenna reflection coefficient, S_{11}, when a small air-gap or a hair layer of varying thickness d is introduced between the antenna and the skin, is shown in Fig. 4. In particular, the hair layer is modelled as suggested in [30], with the dielectric properties and conductivity set equal to $\epsilon_{r-hair} = 1.65$ and conductivity $\sigma = 0.060$ S/m, at 1 GHz. Fig. 4 clearly shows that when there is no perfect contact (with the skin) the antenna's response degrades, especially for the air-gap case. However, in view of the small size of the antenna, performance degradation due to air gaps can be avoided by using some precautions, as in [31], where good contact between antenna and head is ensured by a pneumatic system which controls the movements (toward and away from the head) of each antenna individually. Instead, since in realistic cases hair thickness can be even $t_{hair} = 5$ mm, pressing the antenna against the head helps in reducing hair thickness as well. However, as shown, this continues to negatively impact on the antenna's behaviour.

3. CIRCULAR BRICK ANTENNA DESIGN, REALIZATION AND NUMERICAL RESULTS

In this section, the weaknesses suffered by the HSA when it is placed in contact with the hair are overcome by designing a new antenna. The idea is to equip the antenna with a matching layer, as proposed in [25], which must keep the antenna's performance stable in the cases that it is placed both on the skin and on the hair layer. However, instead of using a solid material, a liquid medium is proposed in order to make the manufacturing process easy and allows for lighter and smaller antennas. More in detail, the coupling medium and the antenna are enclosed in a small cylindrical container. The coupling medium permittivity, the geometry of the container, and the antenna are chosen to be trade-off between the sensor's compactness and, again, a minimum return loss of 10 dB across the operating band $[1, 2]$ GHz. This new antenna is addressed as HCA (head cylindrical antenna) hereafter.

As a starting point, the antenna shown in Fig. 2(b) is re-optimized to work within a coupling medium of permittivity $\epsilon_{r-medium} \approx 25$. In particular, for design procedure, the central frequency ($f_0 = 1.5$ GHz) into the imaging band $[1, 2]$ GHz is considered as the working frequency. Initially, the dimension of the circular container depicted in Fig. 5 is set in order to guarantee a distance of 0.5 times of the wavelength in the coupling medium between the surface of container and the antenna. In order to clarify how the matching layer mitigates the effect of hair and air gap, the transmission line model depicted in Fig. 6 can be exploited. The biological load impedance Z_L is derived according to [17]. At frequency $f_0 = 1.5$ GHz, the wavelength in air/hair material is about 20 cm. Differently, as discussed in previous section, the air gap and the thickness of hair do not exceed 0.5 cm taking some precautions [32]. Accordingly, the thickness layer $d_{AIR/HAIR} < \lambda/10$, hence the overall impedance behaviour Z_{IN} of the resulting equivalent model (see right panel of Fig. 6) is little sensitive towards hair tissue and air gap. Virtually the skin tissue directly touches the coupling media. This greatly simplifies the designed procedure since the matching between the antenna immersed in coupling medium and the head model can be achieved by exploiting a $\lambda_{MEDIUM}/4$ transformer. The final dimensions of HCA together with the cylindrical container are achieved by numerical simulations on the HFSS software taking into account the previous reasoning and the same constraints adopted for HSA. Note that now the area of the front (radiating) part of the HCA is 12.5 cm^2 (diameter about 2 cm), which is slightly larger than the HSA but still has sufficient compact to allow the deployment of many antennas for imaging purposes. Accordingly, the compactness and operative bandwidth constraints are satisfied. The realized prototype of the HCA is shown in Fig. 5(b). It is

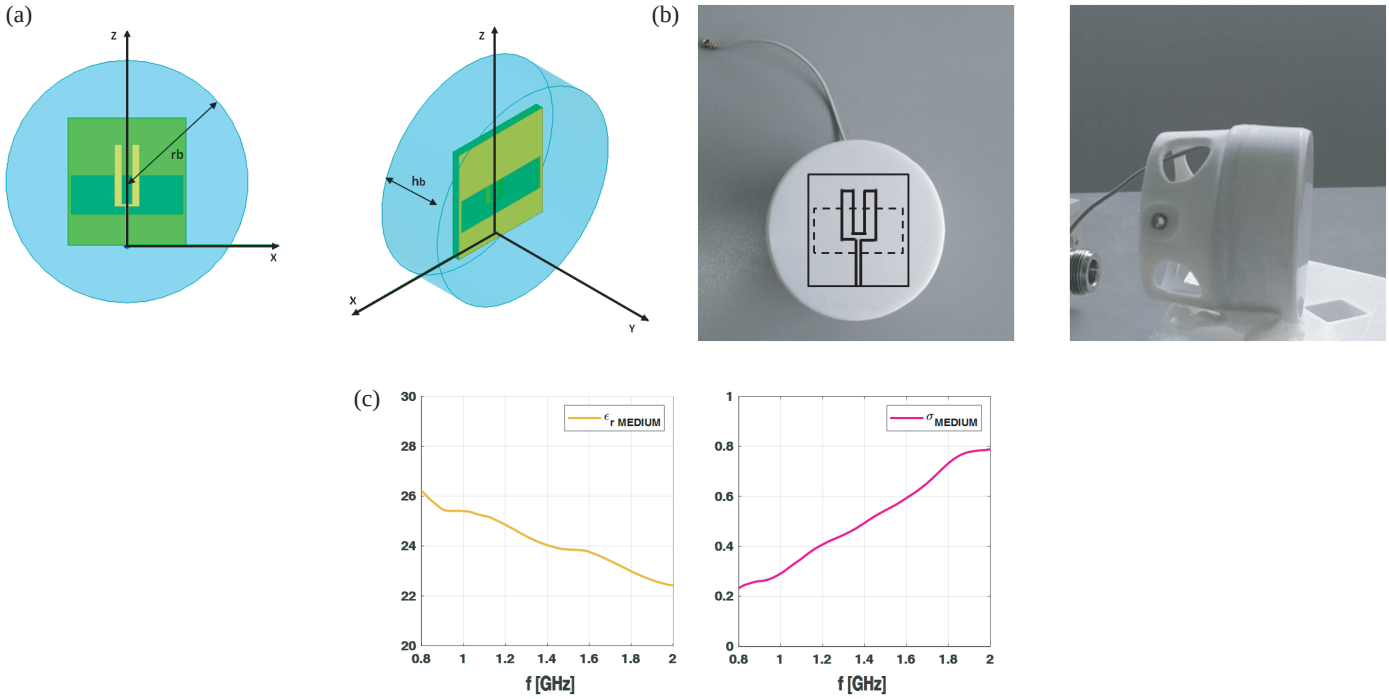

FIGURE 5. HCA. Panel (a) shows antenna geometry and cylindrical container with radius $r_b = 22$ mm and height $h_b = 14$ mm, (b) antenna prototype, and (c) coupling medium dielectric and conductivity as functions of frequency.

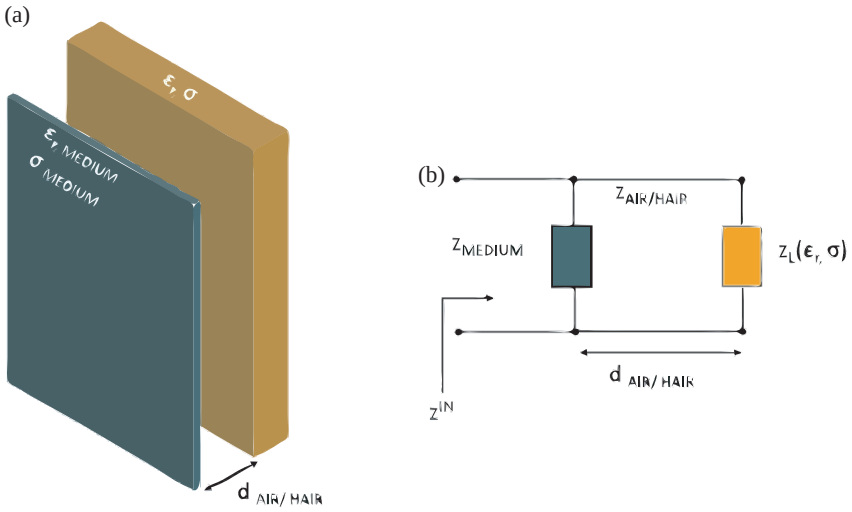

FIGURE 6. Schematic draw depicting the coupling medium adopted to mitigate the hair and air gap effect (a) and the equivalent transmission line TL model (b).

worth remarking that another element is present in the back side of structure. This does not enter the radiation process but gives the antenna additional mechanical stiffness, thus improving the robustness of the device and enabling good bending, as required to cover the head. It is clear that these precautions will allow to realize more easily an array conformal to the head for MWI. The whole circular container is realized by additive manufacturing with a 3-D plastic printer and filled up with a liquid mixture. Indeed, the coupling medium is a liquid obtained from a proper mixture of de-ionized water and Triton X-100 [33]. The corresponding measured dielectric and conductive properties are shown in Fig. 5. To achieve such measurements, a system similar to the one exploited in [34] is used. In particular, the sensor is an open-ended coaxial probe (RG402), and the vector network analyzer adopted is TR1300. A 6 MHz frequency step is used in frequency range of 1 to 3 GHz.

In order to check the HCA response, the numerical phantom of Fig. 3 is once again considered, and the same cases are rerun as in Fig. 4. The corresponding results are reported in Fig. 7. It is possible to clearly observe that, thanks to the coupling medium, the effect of a small air-gap and hair layer is greatly mitigated. Indeed, the HCA S_{11} remains below -10 dB

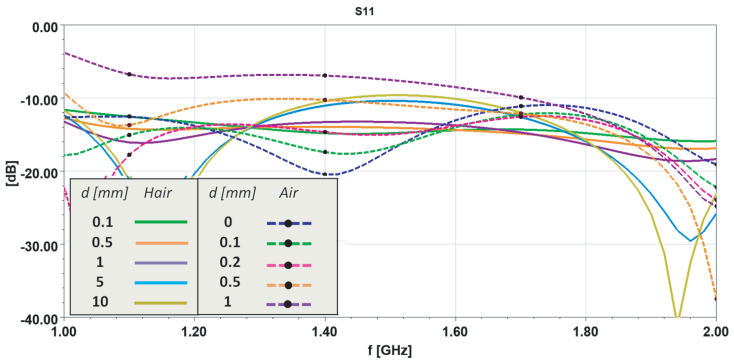

FIGURE 7. Role of hair and air gap. Simulated reflection coefficient amplitude for different air-gaps and hair layer thickness d [mm] between the HCA and complete phantom.

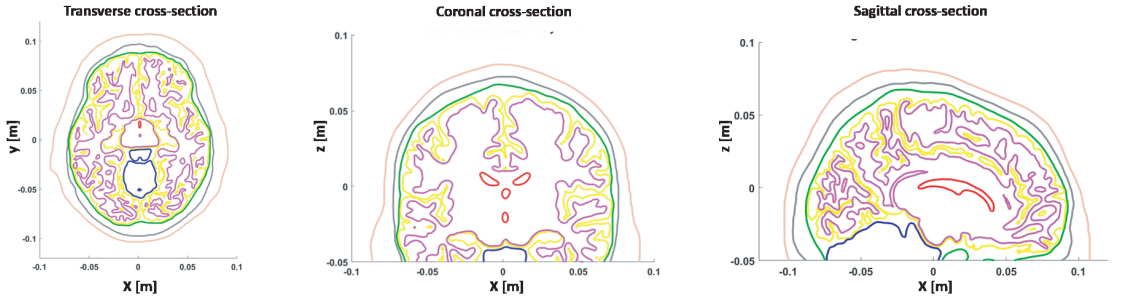

@ 1 GHz	Ventricles	White matter	Cerebellum	Gray matter	CSF	Bone	Skin
ε_r	68.20	38.58	48.85	52.30	68.20	18.00	41.00
σ [S/m]	2.30	0.62	1.31	0.98	2.30	0.40	0.85

FIGURE 8. Cuts of numerical phantom ID110411.

over the working frequency band $[1, 2]$ GHz for all the cases but one. The latter, however, corresponds to the air-gap situation that, as mentioned above, can be avoided if some systems are used to enforce good contact between the antenna and the head. Note that the influence of the hair is mitigated as well, even for the case of hair thickness t_{hair} as large as one centimeter.

4. CHECKING ANTENNAS' RESPONSES AGAINST REALISTIC NUMERICAL PHANTOM

So far, the numerical analysis is carried out for the planar layered simplified head model shown in Fig. 3(a). This allows to focus on how the air gap and hair affect the antennas' responses. In practical cases, the antenna's behaviour can also change due to the head curvature. Therefore, it is necessary to address the case of more realistic head phantoms, which possibly include the typical head tissue layering. To this end, the proposed antenna sensors are simulated when being put in contact to a realistic human head using CST electromagnetic simulator. The 3D anatomically realistic head phantoms (ID110411) are derived from MRI data-sets from [35] and imported in CST. Overall, there are seven tissues with dielectric properties at 1 GHz derived from [29] and summarized in Fig. 8.

The two cases shown in Fig. 9(a) are considered. For the case addressed as scenario A, the antennas are located on the lateral side of the head (indeed symmetrically on the opposite sides), whereas for scenario B, the sensors are placed on head top. In the latter case, since the head is almost flat, a quasi perfect contact is achieved for both sensors. Therefore, a good matching over the operative frequency band is achieved for both the antennas (see panel b). When the sensors are placed symmetrically over the head over opposite sides (scenario A), the antennas' behaviours change. By looking at the scattering parameter S_{11}, it is possible to see that the HCA complies with the design requirements a part for a small frequency range where S_{11} slightly exceeds -10 dB. Conversely, the HSA response is strongly affected by head curvature, especially toward the lower edge of the frequency band. Moreover, the same figure depicts the transmission coefficient S_{21} when two antennas are placed on opposite sides of the head (wide antenna configuration (WAC)). In particular, when a perfect contact between antenna and head surface is considered, the dynamic range of S_{21} parameter is quite similar. Things dramatically change when a small air gap is considered (i.e., $d = 0.25$ mm). In this case, the transmission coefficient S_{21} related to HSA drops abruptly; differently, the same parameter remains rather stable for HCA.

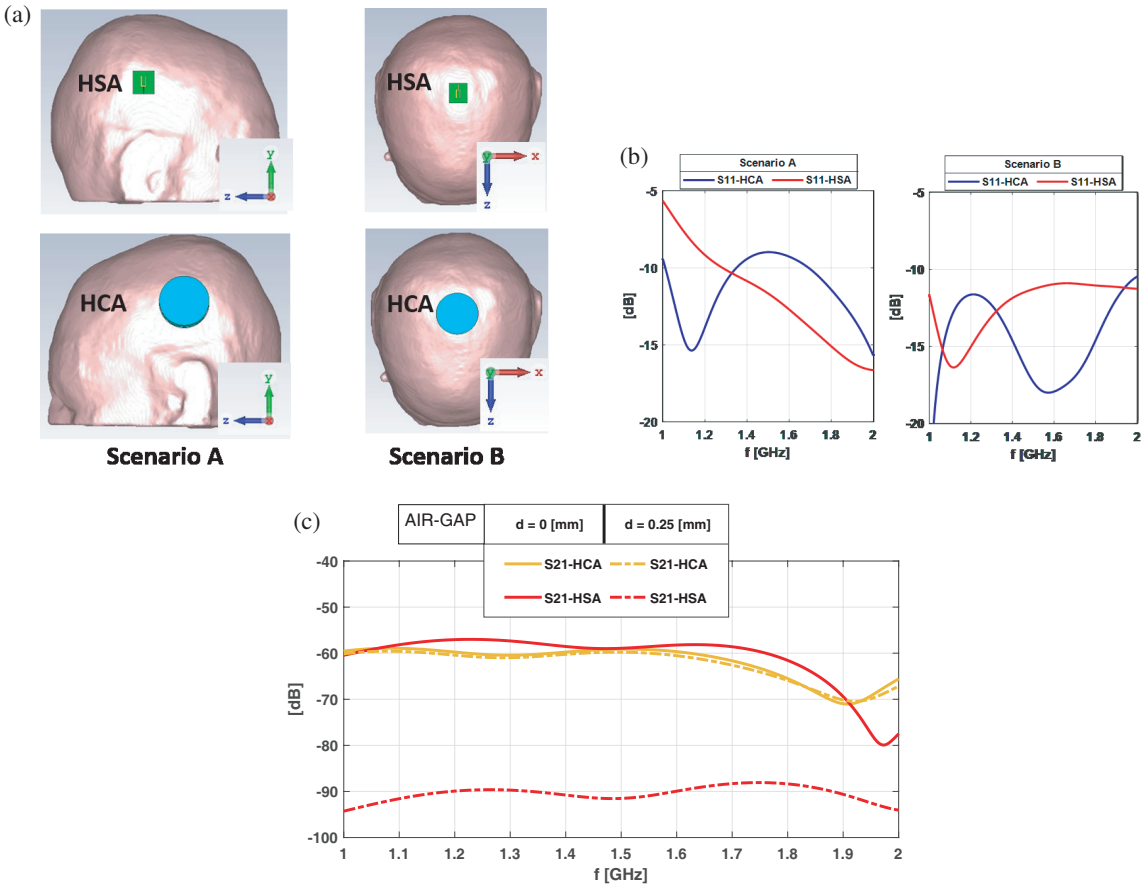

FIGURE 9. Head numerical phantom and antennas' configurations. In Panel (a) HSA and HCA placed in two different head area, (b) scattering parameters S_{11} for both scenarios, and (c) transmission coefficient S_{21} for WAC configuration.

Accordingly, we conclude that the transmission characteristics are affected very little by the loss of coupling media. In Fig. 10, the field distribution into the head phantom at 1 GHz is examined to get insight on the field penetration. As can be seen, even if the HCA does not perfectly adhere to the head surface, it allows for a good penetration depth. Moreover, the field distribution magnitude into head is rather uniform. As opposed, the HSA leads to lower and different field penetrations which strongly depend on antenna positions, especially in the case of scenario A. This can be clearly seen by the looking at the panels on the top row of Fig. 10. Finally, by looking the results shown in Fig. 9(c) and Fig. 10, the attenuation on the radiated field due to lossy coupling media represents a minimal disadvantage compared to the benefits achieved.

5. EXPERIMENTAL RESULTS

In this section, some experimental results are presented by considering only the scattering parameters. Of course, field penetration and distribution inside the head is of great importance as well. However, while these aspects can be easily studied through simulations, as shown above, they are very difficult to analyze through experiments, even by employing phantoms of the head.

Therefore, experiments concern the antenna scattering parameters which are measured with a vector network analyzer (VNA) Copper Mountain TR5048 [36]. A stimulus in frequency band $[1, 2]$ GHz is adopted selecting a step frequency equal to 5 MHz. The power of generated signal P_{out} is fixed to -10 dBm. To actually appreciate the achievable performance of both HSA and HCA, they are measured when being located against a human head. Fig. 11 presents the S_{11} of the HSA and HCA (solid and dashed lines, respectively). Different placements on the head of a human subject are considered. In particular, the position addressed as c_0 refers to the case that the antenna is on the forehead, i.e., in contact with the skin, whereas positions c_1 and c_2 are illustrated in the right panel of the same figure and refer to the locations where there is a different "amount" of hair. When the HSA is placed on the forehead, its S_{11} is similar to the numerical case, staying below -10 dB. However, placement over hair, particularly in position c_2, increases S_{11}, failing to meet design requirements. In contrast, the HCA (dashed lines in the same Figure), despite some variations from numerical cases due to the simplified phantom, consistently meets the design requirements across the entire frequency band for both skin and hair positions (c_0, c_1, and c_2). Thus, it can be concluded that the expected better HCA behaviour is verified under realistic measurement conditions.

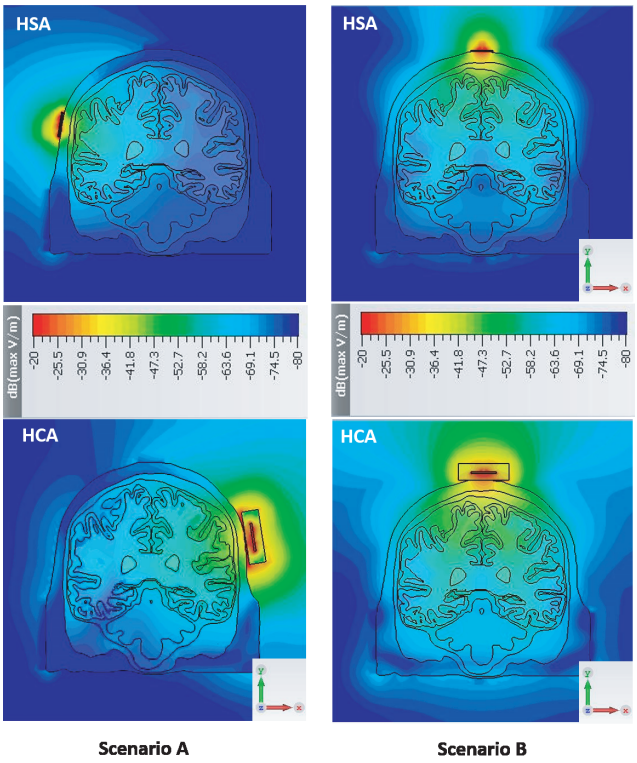

FIGURE 10. Amplitude field $|E|$ distribution at 1 GHz, coronal-view. Left and right panels refers to same cases display in Fig. 9(a).

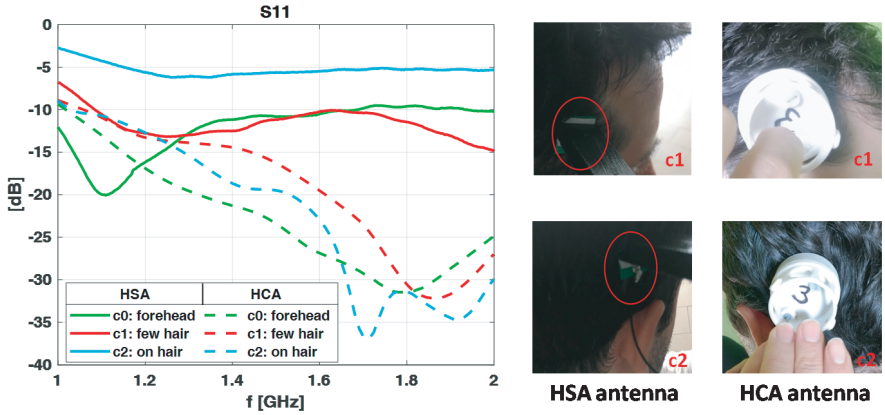

FIGURE 11. Measured scattering parameters with different placements of HSA and HCA on a human head.

Additional experimental results for the HCA are detailed in Fig. 12. Here, the aim is to check the stability of the antenna's response by changing the position on the head (with respect to ones considered in the the previous case) and by considering different subjects under test. To this end, four volunteers are recruited and for each of them two HCA, denoted as antenna A1 and A2 respectively, are located according to two different configurations. The first configuration concerns the two antennas placed on the same side of the head (narrow antenna configuration (NAC)), whereas the second one refers to the two antennas placed on opposite sides of the head (wide antenna configuration (WAC)). Pictures illustrating these experimental configurations are shown in the top part of Fig. 12(a). As a reference, the same case as the experimental configuration is considered for numerical examples. The positions of the antennas against the same numerical phantom, as used in the previous section, are shown again in panel a.

The considered parameters are S_{11}, S_{22}, and S_{21}. In particular, the transmission scattering parameter is included since it is relevant for MWI systems employing multistatic configurations. In these cases, it is crucial to analyze the transmission of the signal through the head, which is linked to the obtainable signal to noise ratio.

In order to evaluate the hair effect, four different real human heads are considered. The volunteers addressed as ID1 and ID2 refer to "regular" hair case; ID4 refers to very short hair case; and finally ID3 is almost hairless. The corresponding measurements are shown in Fig. 12(c), with panels in each row per-

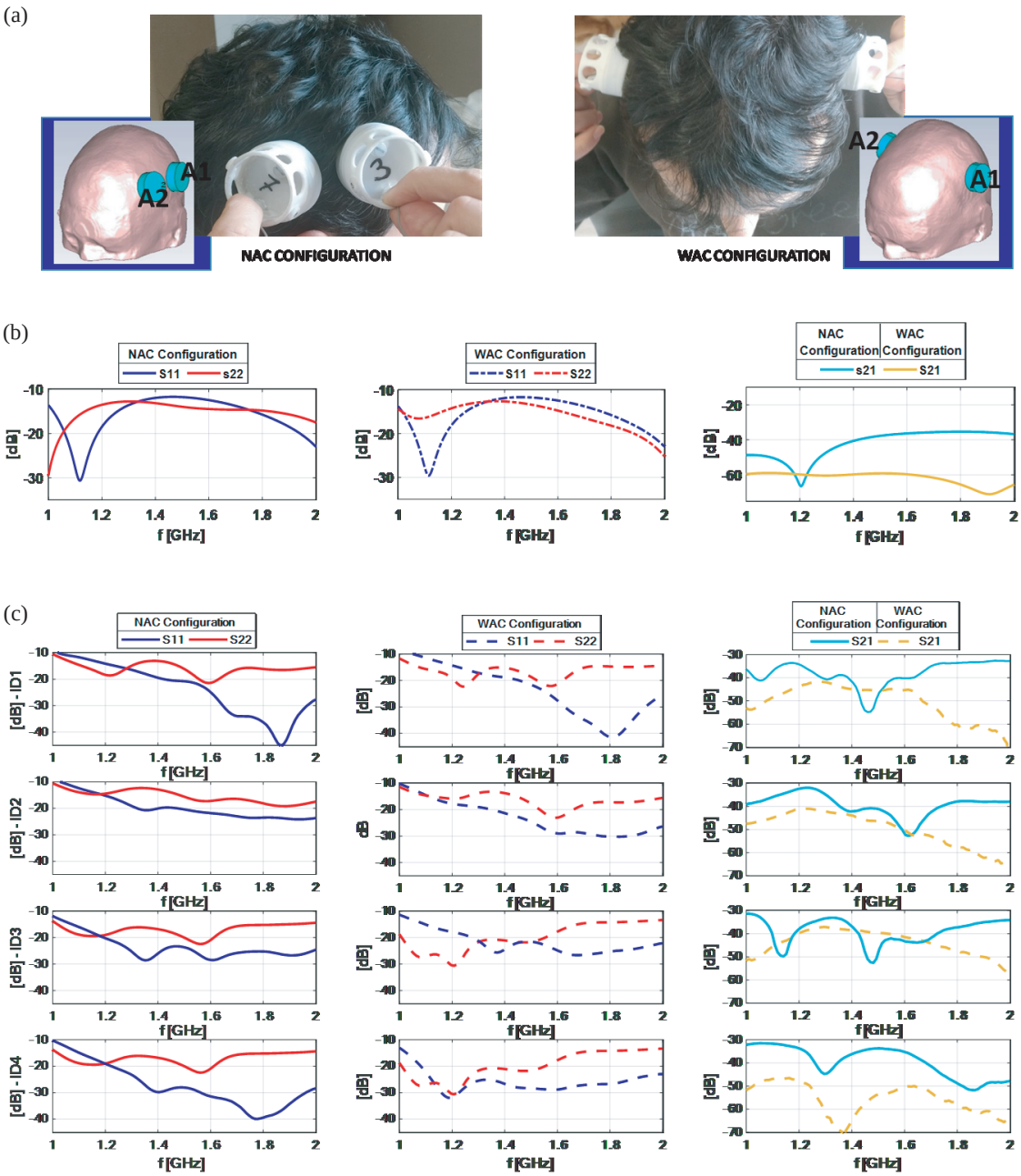

FIGURE 12. HCA. Measured scattering parameters for the NAC and WAC configurations. Panel (a) shows the antennas' configuration for the experiments and for the numerical simulations, (b) the numerical scattering parameters and (c) the measurements corresponding to four volunteers.

TABLE 3. Antenna performance comparison with other related paper.

Ref	Dimensions [mm]	Medium	$\lvert S_{11}\rvert$ < -10 dB	$\lvert S_{21}\rvert$ dB NAC/WAC
Here-HSA	$18 \times 11 \times 1.6$	on body	[1–2] GHz	NA
Here-HCA	22×14	liquid	[1–2] GHz	$-52/-70$
[25]	$50 \times 50 \times 70$	solid	[0.8–1.2] GHz	$-35/-65$
[37]	$50 \times 50 \times 70$	liquid	[0.8–2] GHz	$\mathrm{NA}/-80$
[38]	$40 \times 46 \times 14.4$	on body	[1.2–1.5] GHz	$-25/-50$

taining to a given volunteer, whereas the numerical examples corresponding to a phantom without the hair layer are shown in panel b. It is observable that, for each volunteer, S_{11} and S_{22} are quite stable while passing from the NAC to the WAC configurations. However, the behaviors of the two antennas are different, due to imperfections and tolerance of the manufacturing process. Apart from this aspect, for the scattering parameters the same considerations apply as for the numerical results depicted in the same figure. Finally, Table 3 compares the realized HSA and HCA with respect to other antennas used in other brain MWI devices. Here, it is shown that the frequency band $[1, 2]$ GHz is a shared choice whereas the transmission coefficient S_{21} dynamic is comparable to the values reported in literature.

6. CONCLUSION

We have presented two antennas for brain imaging that operate effectively in direct contact with the head, well matched between 1 and 2 GHz. In particular, it has been shown that while for HSA the air-gap issues can be avoided since the antennas are compact in size, the head curvature negatively affects its performance. Moreover, when passing from the skin to the hair side, the antenna's response degrades dramatically, making the HSA ineffective, which suggests that the hair effect must be taken into account to secure a stable antenna's response. These limitations have been overcome with the proposed HCA that is proven to comply with the design constraints over a 1 GHz frequency band. The HCA shows strong stability under different setup measurement configurations ensuring the matching in frequency band $[1, 2]$ GHz and a satisfactory EM wave penetration inside the head. Moreover, it has small size (circular brick of radius 22 mm and height 14 mm) and the dynamic value of transmission coefficient S_{21} no lower than -70 dB, which is well above the VNA noise floor. Accordingly, the proposed HCA, with its stable performance and suitability for microwave brain imaging, addresses the limitations found in HSA.

REFERENCES

[1] Conceicao, R. C., J. J. Mohr, and M. O'Halloran, *An Introduction to Microwave Imaging for Breast Cancer Detection*, Springer International, Basel, Switzerlan, 2016.

[2] Fear, E. C., P. M. Meaney, and M. A. Stuchly, "Microwaves for breast cancer detection?" *IEEE Potentials*, Vol. 22, No. 1, 12–18, 2003.

[3] Ruvio, G., R. Solimene, A. Cuccaro, G. Fiaschetti, A. J. Fagan, S. Cournane, J. Cooke, M. J. Ammann, J. Tobon, and J. E. Browne, "Multimodal breast phantoms for microwave, ultrasound, mammography, magnetic resonance and computed tomography imaging," *Sensors*, Vol. 20, No. 8, 2400, 2020.

[4] Donelli, M., I. J. Craddock, D. Gibbins, and M. Sarafianou, "A three-dimensional time domain microwave imaging method for breast cancer detection based on an evolutionary algorithm," *Progress In Electromagnetics Research M*, Vol. 18, 179–195, 2011.

[5] Lim, H. B., N. T. T. Nhung, E.-P. Li, and N. D. Thang, "Confocal microwave imaging for breast cancer detection: Delay-multiply-and-sum image reconstruction algorithm," *IEEE Transactions on Biomedical Engineering*, Vol. 55, No. 6, 1697–1704, 2008.

[6] Flores-Tapia, D. and S. Pistorius, "Real time breast microwave radar image reconstruction using circular holography: A study of experimental feasibility," *Medical Physics*, Vol. 40, No. 10, 5420–5431, 2013.

[7] Ruvio, G., A. Cuccaro, R. Solimene, A. Brancaccio, B. Basile, and M. J. Ammann, "Microwave bone imaging: A preliminary scanning system for proof-of-concept," *Healthcare Technology Letters*, Vol. 3, No. 3, 218–221, 2016.

[8] Yilmaz, T., R. Foster, and Y. Hao, "Broadband tissue mimicking phantoms and a patch resonator for evaluating noninvasive monitoring of blood glucose levels," *IEEE Transactions on Antennas and Propagation*, Vol. 62, No. 6, 3064–3075, 2014.

[9] Crocco, L., I. Karanasiou, M. L. James, and R. C. Conceicao, *Emerging Electromagnetic Technologies For Brain Diseases Diagnostics, Monitoring and Therapy*, Springer International, Cham, Switzerland, 2018.

[10] Li, X., E. J. Bond, B. D. V. Veen, and S. C. Hagness, "An overview of ultra-wideband microwave imaging via space-time beamforming for early-stage breast-cancer detection," *IEEE Antennas and Propagation Magazine*, Vol. 47, No. 1, 19–34, 2005.

[11] Sharma, M. K., M. Kumar, J. P. Saini, D. Gangwar, B. K. Kanaujia, S. P. Singh, and A. Ekuakille, "Experimental investigation of the breast phantom for tumor detection using ultra-wide band-mimo antenna sensor (UMAS) probe," *IEEE Sensors Journal*, Vol. 20, No. 12, 6745–6752, 2020.

[12] Li, X., L. Zwirello, M. Jalilvand, and T. Zwick, "Design and near-field characterization of a planar on-body UWB slot-antenna for stroke detection," in *2012 IEEE International Workshop on Antenna Technology (iWAT)*, 201–204, Tucson, AZ, USA, 2012.

[13] Elyassi, R. and G. Moradi, "Flexible and moon-shaped slot UWB implantable antenna design for head implants," *International Journal of Microwave and Wireless Technologies*, Vol. 9, No. 8, 1559–1567, 2017.

[14] Rana, B., J.-Y. Shim, and J.-Y. Chung, "An implantable antenna with broadside radiation for a brain-machine interface," *IEEE Sensors Journal*, Vol. 19, No. 20, 9200–9205, 2019.

[15] Zamani, A., A. M. Abbosh, and A. T. Mobashsher, "Fast frequency-based multistatic microwave imaging algorithm with application to brain injury detection," *IEEE Transactions on Microwave Theory and Techniques*, Vol. 64, No. 2, 653–662, 2016.

[16] Lei, W., L. Xu, X. Jiang, J. Luo, and F. Hou, "Automatic recognition of basic strokes based on FMCW radar system," *IEEE Sensors Journal*, Vol. 21, No. 13, 15 101–15 113, 2021.

[17] Scapaticci, R., L. D. Donato, I. Catapano, and L. Crocco, "A feasibility study on microwave imaging for brain stroke monitoring," *Progress In Electromagnetics Research B*, Vol. 40, 305–324, 2012.

[18] Ruvio, G., R. Solimene, A. Cuccaro, and M. J. Ammann, "Field penetration in mri-based breast models: A numerical investigation," in *The 8th European Conference on Antennas and Propagation (EUCAP 2014)*, 316–319, The Hague, Netherlands, 2014.

[19] Sugitani, T., S. Kubota, A. Toya, X. Xiao, and T. Kikkawa, "A compact 4×4 planar UWB antenna array for 3-D breast cancer detection," *IEEE Antennas and Wireless Propagation Letters*, Vol. 12, 733–736, 2013.

[20] Li, X., M. Jalilvand, Y. L. Sit, and T. Zwick, "A compact double-layer on-body matched bowtie antenna for medical diagnosis," *IEEE Transactions on Antennas and Propagation*, Vol. 62, No. 4, 1808–1816, 2014.

[21] Bashri, M. S. R., T. Arslan, W. Zhou, and N. Haridas, "Wearable device for microwave head imaging," in *2016 46th European Microwave Conference (EuMC)*, 671–674, London, UK, 2016.

[22] Roshani, S., S. Koziel, S. I. Yahya, M. A. Chaudhary, Y. Y. Ghadi, S. Roshani, and L. Golunski, "Mutual coupling reduction in antenna arrays using artificial intelligence approach and inverse neural network surrogates," *Sensors*, Vol. 23, No. 16, 7089, 2023.

[23] Mirza, A. F., C. H. See, I. M. Danjuma, R. Asif, R. A. Abd-Alhameed, J. M. Noras, R. W. Clarke, and P. S. Excell, "An active microwave sensor for near field imaging," *IEEE Sensors Journal*, Vol. 17, No. 9, 2749–2757, 2017.

[24] Cuccaro, A., A. Dell'Aversano, G. Ruvio, J. Browne, and R. Solimene, "Incoherent radar imaging for breast cancer detection and experimental validation against 3D multimodal breast phantoms," *Journal of Imaging*, Vol. 7, No. 2, 23, 2021.

[25] Rodriguez-Duarte, D. O., J. A. T. Vasquez, R. Scapaticci, L. Crocco, and F. Vipiana, "Brick-shaped antenna module for microwave brain imaging systems," *IEEE Antennas and Wireless Propagation Letters*, Vol. 19, No. 12, 2057–2061, 2020.

[26] Croswell, W., R. Rudduck, and D. Hatcher, "The admittance of a rectangular waveguide radiating into a dielectric slab," *IEEE Transactions on Antennas and Propagation*, Vol. 15, No. 5, 627–633, 1967.

[27] Jones, J., "The influence of air-gap tolerances on the admittance of a dielectric-coated slot antenna," *IEEE Transactions on Antennas and Propagation*, Vol. 17, No. 1, 63–68, 1969.

[28] Deschamps, G., "Impedance of an antenna in a conducting medium," *IRE Transactions on Antennas and Propagation*, Vol. 10, No. 5, 648–650, 1962.

[29] Gabriel, S., R. Lau, and C. Gabriel, "The dielectric properties of biological tissues: III. Parametric models for the dielectric spectrum of tissues," *Physics in Medicine & Biology*, Vol. 41, No. 11, 2271–2293, 1996.

[30] You, K. Y. and Y. L. Then, "Electrostatic and dielectric measurements for hair building fibers from DC to microwave frequencies," *International Journal of Medical and Health Sciences*, Vol. 9, No. 3, 312–319, 2015.

[31] Solimene, R., B. Basile, J. Browne, A. Cuccaro, A. Dell'Aversano, and G. Ruvio, "An incoherent radar imaging system for medical applications," in *2021 IEEE Conference on Antenna Measurements & Applications (CAMA)*, 493–498, Antibes Juan-les-Pins, France, 2021.

[32] Cuccaro, A., A. Dell'Aversano, B. Basile, M. A. Maisto, and R. Solimene, "Subcranial encephalic temnograph-shaped helmet for brain stroke monitoring," *Sensors*, Vol. 24, No. 9, 2887, 2024.

[33] Joachimowicz, N., B. Duchêne, C. Conessa, and O. Meyer, "Anthropomorphic breast and head phantoms for microwave imaging," *Diagnostics*, Vol. 8, No. 4, 85, 2018.

[34] Marsland, T. P. and S. Evans, "Dielectric measurements with an open-ended coaxial probe," *IEE Proceedings H (Microwaves, Antennas and Propagation)*, Vol. 134, No. 4, 341–349, 1987.

[35] [Online]. Available: https://www.nevaelectromagnetics.com/high-resolution-head-models.

[36] [Online]. Available: https://coppermountaintech.com.

[37] Tobon Vasquez, J. A., R. Scapaticci, G. Turvani, G. Bellizzi, N. Joachimowicz, B. Duchene, E. Tedeschi, M. R. Casu, L. Crocco, and F. Vipiana, "Design and experimental assessment of a 2d microwave imaging system for brain stroke monitoring," *International Journal of Antennas and Propagation*, Vol. 2019, No. 1, 8065036, 2019.

[38] Persson, M., A. Fhager, H. D. Trefná, Y. Yu, T. McKelvey, G. Pegenius, J.-E. Karlsson, and M. Elam, "Microwave-based stroke diagnosis making global prehospital thrombolytic treatment possible," *IEEE Transactions on Biomedical Engineering*, Vol. 61, No. 11, 2806–2817, 2014.